Robotica: page 1 of 15. © Cambridge University Press 2011
doi:10.1017/S0263574711000415

Design of a controller for trajectory tracking for compliant mechanisms with effective vibration suppression

P. Boscariol and V. Zanotto*

Dipartimento di Ingegneria Elettrica, Gestionale e Meccanica Università di Udine, Via delle Scienze 208, 33100 Udine, Italy

(Received in Final Form: March 22, 2011)

SUMMARY
In this paper, a numerical investigation of the Model Predictive Control strategy applied to flexible-link mechanisms is presented. The mechanisms used for all the tests are a planar five-link mechanisms. The tests are aimed at showing how the proposed control system can be used for the trajectory tracking and the vibration suppression. An analysis of the effects of the choice of tuning parameters is presented as well. The design of the predictive controller is based on a linearized version of an accurate nonlinear dynamic model. The effectiveness of the proposed approach is confirmed by extensive numerical results.

KEYWORDS: Vibration; Robotics; Flexible link; Trajectory; Dynamics; Mechatronic systems; Control of robotic systems.

1. Introduction

Modeling and the control of flexible-link mechanisms are fundamental topics in robotics engineering. Severe vibrations due to inertial components of the motion arise in manipulators when they are exposed to large accelerations. If neglected, these dynamic effects can lead to major worsening of accuracy, mechanical failures, and instability.[1] The complexity of the problem is very high when dealing with both modeling and control since an accurate description of the dynamics in multilink flexible mechanism requires complex and nonlinear models.[2] The problem is even more challenging when trajectory tracking in the operational space is required since the requirements on accuracy are even much stricter.

As far as the modeling of multilink flexible mechanism is concerned, many different solutions have been proposed in the last 40 years. A comprehensive review can be found in ref. [2]. Among the different approaches, Finite Element Method (FEM) has been the most popular. This approach, which is based on the discretization of elastic deformation into a finite set of nodal displacements, has been used in refs. [3, 4]. Some authors have also proposed a description of flexible-link mechanisms making use of modal coordinates in places of physical coordinates.[5,6] Further approaches can be found in refs. [7, 8]. The majority of works has been conducted on single-link flexible mechanism[9,10] and multibody systems with only one flexible link, as in refs. [11, 12]. In refs. [13] and [14], the authors deal with multibody flexible mechanisms: in the former, a regulator for controlling a three Degrees Of Freedom (DOFs) planar manipulator with two flexible links is presented, while the latter concerns a two planar cooperating three-link flexible robot with payload.

The aim of this paper is to investigate the effectiveness of the Model-based Predictive Control (MPC) strategy for trajectory tracking and vibration control in multilink flexible mechanism with two rigid DOFs, in order to extend the results already developed by the same authors in refs. [21, 22] and to further develop a new branch of research. MPC refers to a family of control algorithms that compute the optimal control sequence based on the knowledge of the plant and the feedback information. This information, together with a set of constraints, is used as the basis of an optimization problem. The use of MPC to control vibration in mechanisms has been investigated in a limited number of scientific papers. For example, MPC controller has been applied to the vibration control of a simple structure in ref. [15], while vibration control in different mechanisms has been presented in refs. [16–18]. Again, on the subject of predictive control for flexible-link mechanisms, even less papers have been written: to authors' knowledge the only papers focusing on this subjects are.[19–22] In refs. [19–21], predictive control strategies have been used to control the position and the vibrations of a single-link mechanism, while in ref. [22] a constrained MPC has been applied as a position regulator to a four-link closed-chain flexible-link mechanism. The choice of this control strategy has been motivated by different factors. First, the prediction ability based on an internal model can be a very effective tool in fast-dynamic systems. Then, MPC is well suited to Multiple-Inputs–Multiple-Outputs (MIMO) systems since the outputs are computed by solving a minimization problem, which takes account of different variables.

This work is meant to be an extension of previously published works[21,22] in the wake of the very good results obtained trough predictive control action. The mechanism under investigation in this paper is a five-link planar mechanisms, with flexibility distributed in all the links. The previous papers are focused on a single-link[21] and a four-link mechanism.[22] For this reason, this paper investigates the behavior of a multiactuated Flexible-Link Manipulator (FLM). The presence of two rigid DOFs allows to study the response of the closed-loop systems for bidimensional

* Corresponding author. E-mail: vanni.zanotto@uniud.it

trajectory tracking problems. In particular, the tracking in both the operational and joint space is being investigated in this work. This is a problem of high interest since it is well known that a system that performs a good tracking in the joint space will not necessarily perform with sufficient accuracy in the operational space, i.e., the motion of the end effector could be inaccurate.[1] A major worsening of the end-effector trajectory tracking can be caused by a less than sufficient synchronization between the motion of the two axis. The effects of the *reference-lookahead* are here investigated to evaluate how this technique can improve the accuracy of the closed-loop system. Moreover, the effects of the choice of different interpolating function for the trajectory planning of the end effector are investigated. None of the cited papers deals with the aspects highlighted here.

This paper is organized as follows: the nonlinear dynamic model of the flexible-link mechanism is briefly introduced in Section 2. Section 3 provides a description of the mechanism available in the Mechatronics Laboratory at the Faculty of Engineering, University of Udine (Italy). In the last part of the Section 3, the state observer employed in the closed-loop system is shown, together with some numerical results that demonstrate its accuracy. A description of the predictive control strategy is reported in Section 4, while a detailed report of different simulation results can be found in Sections 5 and 6. In Section 5, the MPC controller is used to simultaneously control the vibration and track a reference signal in the joint spaces. The effects of the reference lookahead strategy are shown, together with some results of the controller robustness to plant parametric mismatches and noises. The effects of different choices of the control tuning parameters are investigated as well. Section 6 deals extensively with the problem of trajectory tracking in the operational space. The effectiveness of the controller during high speed motion is investigated by means of exhaustive simulations. The effects of different choices of tuning parameters and trajectory planning strategies are investigated. The results presented here were obtained trough numerical simulation, using the MATLAB/Simulink environment.

2. Dynamic Model of a Five-Link Planar Mechanism

In this section, the dynamic model of flexible-link mechanisms proposed by Giovagnoni[4] will be briefly explained. The choice of this formulation among the several proposed in the last 40 years has been motivated mainly by the high level of accuracy allowed by this model, which has been proved several times, for example, in refs. [23, 24].

The main characteristics of this model can be summarized in four points:

(1) FEM formulation.
(2) Equivalent Rigid-Link System (ERLS) formulation.
(3) Mutual dependence of rigid and flexible motion.
(4) Suitability to mechanisms with an arbitrary number of both flexible and rigid links.

Each flexible link belonging to the mechanism is subdivided into finite elements. The motion of the mechanism can be thought as the superposition of the motion of an ERLS and the elastic motion of the nodes of the finite elements. Therefore, the free coordinates of the system are the angular position of the two cranks (vector $\mathbf{q}$) and the vector of the nodal displacements $\mathbf{u}$. The dynamic equations of motions are

Table I. Nomenclature used in Eq. (1).

Symbol	Description
$\mathbf{q}$	vector of the free coordinates
$\mathbf{u}$	vector of nodal displacements
$\mathbf{M}$	mass matrix
$\mathbf{K}$	stiffness matrix
$\mathbf{S}$	sensitivity coefficient matrix
$\mathbf{I}$	identity matrix
$\mathbf{M}_G$	matrix of Coriolis acceleration contributions
$\mathbf{g}$	vector of gravity forces
τ	vector of external forces
α, β	Rayleigh damping constants

$$\begin{bmatrix} \mathbf{M} & \mathbf{MS} & \mathbf{0} & \mathbf{0} \\ \mathbf{S}^{\mathrm{T}}\mathbf{M} & \mathbf{S}^{\mathrm{T}}\mathbf{MS} & \mathbf{0} & \mathbf{0} \\ \mathbf{0} & \mathbf{0} & \mathbf{I} & \mathbf{0} \\ \mathbf{0} & \mathbf{0} & \mathbf{0} & \mathbf{I} \end{bmatrix} \begin{bmatrix} \ddot{\mathbf{u}} \\ \ddot{\mathbf{q}} \\ \dot{\mathbf{u}} \\ \dot{\mathbf{q}} \end{bmatrix} = \begin{bmatrix} \mathbf{M} & \mathbf{I} \\ \mathbf{S}^{\mathrm{T}}\mathbf{M} & \mathbf{S}^{\mathrm{T}} \\ \mathbf{0} & \mathbf{0} \\ \mathbf{0} & \mathbf{0} \end{bmatrix} \begin{bmatrix} \mathbf{g} \\ \tau \end{bmatrix}$$
$$+ \begin{bmatrix} -2\mathbf{M}_G - \alpha\mathbf{M} - \beta\mathbf{K} & -\mathbf{M}\dot{\mathbf{S}} & -\mathbf{K} & \mathbf{0} \\ \mathbf{S}^{\mathrm{T}}(-2\mathbf{M}_G - \alpha\mathbf{M}) & -\mathbf{S}^{\mathrm{T}}\mathbf{M}\dot{\mathbf{S}} & \mathbf{0} & \mathbf{0} \\ \mathbf{I} & \mathbf{0} & \mathbf{0} & \mathbf{0} \\ \mathbf{0} & \mathbf{I} & \mathbf{0} & \mathbf{0} \end{bmatrix} \begin{bmatrix} \dot{\mathbf{u}} \\ \dot{\mathbf{q}} \\ \mathbf{u} \\ \mathbf{q} \end{bmatrix} \quad (1)$$

in which $\mathbf{g}$ and τ are the vector of gravitational forces and the vector of external forces, respectively. It should be pointed out that in this model the mentioned rigid and elastic motions are totally coupled each other. The nomenclature employed in Eq. (1) is reported in Table I. For a more detailed description, see ref. [4].

3. Five-Links Mechanism

The mechanism under consideration is the two DOFs manipulator carried out at the Mechatronics Laboratory, Faculty of Engineering, University of Udine, Italy. It is made up of four steel rods connected in a closed-loop chain by using five revolute joints. The motion of the cranks (namely, the first and the fourth link counting anticlockwise) is governed by two torque-controlled actuators. The fifth link (i.e., the chassis) can be considered to be perfectly rigid without affecting the accuracy of the model. The mechanical characteristics of the mechanism are shown in Table II. As it can be seen, the links are very thin (their square section is just 6 mm wide) so the whole mechanism is quite prone to vibration.

The longest links, i.e., the second and the third counting in anticlockwise direction, have been modeled with two Euler–Bernoulli element beam each. The other two flexible elements are described by a single beam element. Every single beam element has six elastic DOFs, so its elastic behavior is completely described by six nodal displacements.

Table II. Kinematic an dynamic characteristics of the flexible-link mechanism.

	symbol	value
Young's modulus	E	200×10^9 Pa
Flexural inertia moment	J	1.08×10^{-10} m^4
Beams width	a	6×10^{-3} m
Beams thickness	b	6×10^{-3} m
Mass/unit of length of links	m	0.282 kg/m
Length of first link	L_1	0.3 m
Length of second link	L_2	0.6 m
Length of third link	L_3	0.6 m
Length of fourth link	L_4	0.3 m
Ground length	L_5	0.3 m
Rayleigh damping constants	α	8.72×10^{-2} s^{-1}
	β	2.1×10^{-5} s

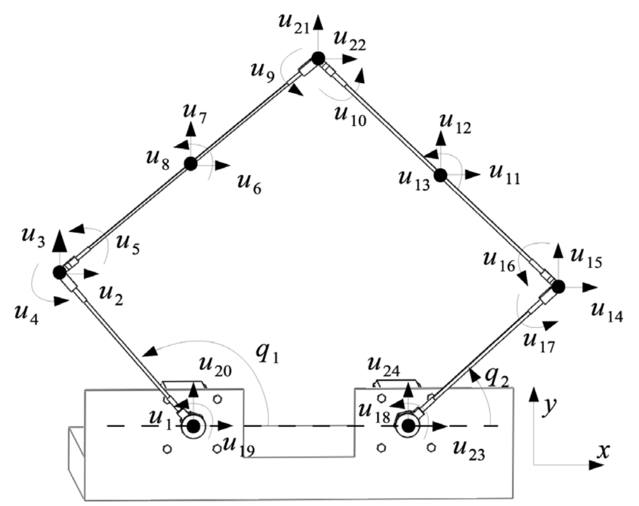

Fig. 1. Elastic displacements and angular position in the five-link mechanism.

On the other hand, the links discretized with two beams have nine DOFs. Considering the continuity between nodal displacements, the overall number of elastic DOFs is 24, as it can be seen in Fig. 1. Four of them ($[u_{19}, u_{20}, u_{23}, u_{24}]$) must be forced to zero to take into account the rigidity of the chassis. Other two displacements must be forced to zero, in order to solve Eq. (1), as explained in ref. [4]. With this choice of finite element discretization, the motion of the mechanism is described by 18 nodal elastic displacements ($\mathbf{u} = [u_1, u_2, \ldots, u_{18}]^{\mathrm{T}}$) and two rigid DOFs ($\mathbf{q} = [q_1, q_2]^{\mathrm{T}}$). A larger number of finite elements could have been used, but at the cost of increasing the computational cost required to perform the simulation and compute the control sequence.

3.1. *Linearized model*

The dynamic model in Eq. (1) is nonlinear since matrix $\dot{\mathbf{S}}$ contains the values of the velocities $\dot{\mathbf{q}}$ of the free coordinates (i.e. $\dot{\mathbf{S}} = \dot{\mathbf{S}}(\dot{\mathbf{q}}, \mathbf{q})$), which yield a quadratic term $\dot{\mathbf{q}}^2$ in the velocities of the free coordinates.[25] As such, it cannot be used as a prediction model for linear MPC controllers. In order to obtain a linear version of the dynamic system, the linearization procedure developed by Gasparetto in ref. [25] has been followed. From the basics of system theory, a linear time-invariant proper model expressed in state-space form can be written as

$$\begin{cases} \dot{\mathbf{x}}(t) = \mathbf{F}_{lin}\mathbf{x}(t) + \mathbf{G}_{lin}\mathbf{w}(t) \\ \mathbf{y}(t) = \mathbf{H}_{lin}\mathbf{x}(t), \end{cases} \tag{2}$$

where $\mathbf{x}(t)$ is the state vector; $\mathbf{y}(t)$ is the output vector; $\boldsymbol{w}(t)$ represents the input vector; and $\mathbf{F}_{lin}$, $\mathbf{G}_{lin}$, and $\mathbf{H}_{lin}$ are time-invariant matrices. The feedthrough term has been neglected in Eq. (13) since the output of the system is simply a linear combination of the state vector.

The input $\mathbf{w}(t)$ for the system is a vector that includes the torques applied to the first and the fourth link: $\mathbf{w}(t) = [\tau_1, \tau_2]^{\mathrm{T}}$. The state vector is $\mathbf{x}(t) = [\dot{u}_1, \ldots, \dot{u}_{18}, \dot{q}_1, \dot{q}_2, u_1, \ldots, u_{18}, q_1, q_2]^{\mathrm{T}}$. The output vector is $\mathbf{y}(t) = [u_1, u_{18}, q_1, q_2]^{\mathrm{T}}$ since this is the subset of the state that is available to the control system as measured variables. In practical applications, u_1 and u_{18} are measured by means of strain gauges, while q_1 and q_2 can be measured by using rotary encoders.

Equation (1) can be written in the following form:

$$\mathbf{A}(\mathbf{q}, \dot{\mathbf{q}}, t)\dot{\mathbf{x}}(t) = \mathbf{B}(\mathbf{q}, \dot{\mathbf{q}}, t)\mathbf{x}(t) + \mathbf{C}(\mathbf{q}, \dot{\mathbf{q}}, t)\mathbf{w}(t) \tag{3}$$

to point out that the matrices involved in Eq. (1) are time-variant and they depend also on $\mathbf{q}$ and $\dot{\mathbf{q}}$, i.e., the position and the velocity of the DOFs. Matrices $\mathbf{A}(\mathbf{q}, \dot{\mathbf{q}}, t)$, $\mathbf{B}(\mathbf{q}, \dot{\mathbf{q}}, t)$, and $\mathbf{C}(\mathbf{q}, \dot{\mathbf{q}}, t)$ can be linearized around an equilibrium point $\mathbf{x}_e$, yielding from Eq. (1) to Eq. (4)

$$\mathcal{A}_{lin}\dot{\mathbf{x}}(t) = \mathcal{B}_{lin}\mathbf{x}(t) + \mathcal{C}_{lin}\mathbf{w}(t). \tag{4}$$

After some steps that can be found in detail in ref. [25], $\mathcal{A}_{lin}$ and $\mathcal{B}_{lin}$ in Eq. (4) can be written as

$$\mathcal{A}_{lin} = \begin{bmatrix} \mathbf{M} & \mathbf{MS} & \mathbf{0} & \mathbf{0} \\ \mathbf{S}^{\mathrm{T}}\mathbf{M} & \mathbf{S}^{\mathrm{T}}\mathbf{MS} & \mathbf{0} & \mathbf{0} \\ \mathbf{0} & \mathbf{0} & \mathbf{I} & \mathbf{0} \\ \mathbf{0} & \mathbf{0} & \mathbf{0} & \mathbf{I} \end{bmatrix}_{\mathbf{x}=\mathbf{x_e}}, \tag{5}$$

$$\mathcal{B}_{lin} = \begin{bmatrix} -2\mathbf{M}_G - \alpha\mathbf{M} - \beta\mathbf{K} & \mathbf{0} & -\mathbf{K} & \mathbf{0} \\ \mathbf{S}^{\mathrm{T}}(-2\mathbf{M}_G - \alpha\mathbf{M} - \beta\mathbf{K}) & \mathbf{0} & \mathbf{0} & \mathbf{0} \\ \mathbf{I} & \mathbf{0} & \mathbf{0} & \mathbf{0} \\ \mathbf{0} & \mathbf{I} & \mathbf{0} & \mathbf{0} \end{bmatrix}_{\mathbf{x}=\mathbf{x_e}}, \tag{6}$$

$$\mathcal{C}_{lin} = \begin{bmatrix} \mathbf{I} \\ \mathbf{S}^{\mathrm{T}} \\ \mathbf{0} \\ \mathbf{0} \end{bmatrix}_{\mathbf{x}=\mathbf{x_e}}. \tag{7}$$

In the previous equations, the symbol $[\cdot]_{\mathbf{x}=\mathbf{x_e}}$ means that the matrices involved in these formulas, which depend on $\mathbf{x}$, are evaluated in the configuration described by $\mathbf{x} = \mathbf{x_e}$. So, Eq. (2) can be rewritten in terms of $\mathcal{A}_{lin}$, $\mathcal{B}_{lin}$, and $\mathcal{C}_{lin}$ as

$$\begin{cases} \dot{\mathbf{x}}(t) = \mathcal{A}_{lin}^{-1}\mathcal{B}_{lin}\mathbf{x}(t) + \mathcal{A}_{lin}^{-1}\mathcal{C}_{lin}\mathbf{w}(t) \\ \mathbf{y}(t) = H_{lin}\mathbf{x}(t). \end{cases} \tag{8}$$

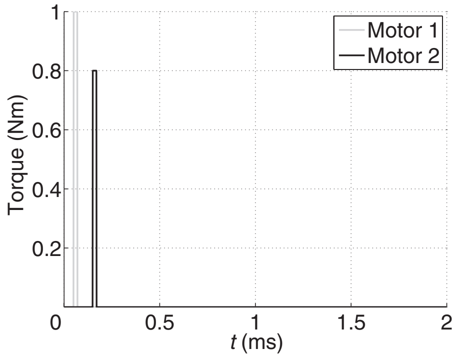

Fig. 2. Torques applied to derive plots in Figs. 3–5.

3.2. State observer

As it will be explained in the next sections, the algorithm used by the MPC requires the whole state vector $\mathbf{x}$ be available at every iteration of the controller. Since in practical situations it is impossible to measure all the 18 nodal displacements that belong to the state vector, a state observer must be used. Here, a Kalman asymptotic estimator has been used. An estimation of $\mathbf{x}(k)$ and $\mathbf{x}_m(k)$ (where $\mathbf{x}(k)$ is the state of the plant model and $\mathbf{x}_m(k)$ is the state of the measurement noise model) can be computed from the measured output $\mathbf{y}(k)$ through

$$\begin{cases} \begin{bmatrix} \hat{\mathbf{x}}(k|k) \\ \hat{\mathbf{x}}_m(k|k) \end{bmatrix} = \begin{bmatrix} \hat{\mathbf{x}}(k|k-1) \\ \hat{\mathbf{x}}_m(k|k-1) \end{bmatrix} + \mathcal{M}(\mathbf{y}(k) - \hat{\mathbf{y}}(k)) \\ \begin{bmatrix} \hat{\mathbf{x}}(k+1|k) \\ \hat{\mathbf{x}}_m(k+1|k) \end{bmatrix} = \begin{bmatrix} \mathbf{F}_{lin}\hat{\mathbf{x}}(k|k) + \mathbf{F}_w\mathbf{w}(k) \\ \tilde{\mathbf{F}}\hat{\mathbf{x}}_m(k|k) \end{bmatrix} \\ \hat{\mathbf{y}}(k) = \mathbf{H}_{lin}\hat{\mathbf{x}}(k|k-1). \end{cases} \quad (9)$$

The $\hat{\cdot}(t_1|t_2)$ symbol represents the estimation of value that will be assumed by the variable under consideration at time t_1 using its value at time t_2. $\mathcal{M}$ is the gain matrix of the observer, while $\mathbf{F}_w$ and $\tilde{\mathbf{F}}$ represent the measurement noise model of the plant.

$\mathcal{M}$, $\mathbf{F}_w$, $\tilde{\mathbf{F}}$ have been designed using Kalman filtering techniques. In this way, the state observer can give an accurate estimation of the full state $\mathbf{x}$ from the knowledge of u_1, u_{18}, q_1, and q_2. This observer presents a very high level of accuracy: some results that prove its performances are shown in Figs. 3–5. The results shown in this graph have been derived by stimulating the nonlinear plant with the impulsive torques, as shown in Fig. 2. These graphs compare the actual nodal displacement and angular positions with their estimated values.

Here, the results are shown only for two rigid rotations and one nodal displacement, but the likeness holds also for all the other nodal displacements belonging to the state vector.

4. Constrained Model Predictive Control

Constrained MPC control is based on these three basic ideas:

- Receding horizon strategy.
- Internal prediction model.
- Constraints on both control and controlled variables.

In this section, a very brief explanation of mentioned concepts is given.[26–28]

4.1. Receding horizon strategy

Here, a single-input–single-output plant will be taken as a matter of example, but the formulation used can be applied without additional efforts to the MIMO case as well. Defining k as the discrete time variable, $y(k)$ and $s(k)$ are the current plant output and the current set-point value, respectively, while $w(k)$ is the plant input value. Then, a reference trajectory $r(k|t)$ can be defined as the ideal trajectory the plant should follow starting from $y(k)$ to reach optimally the set-point trajectory $s(k)$. $r(k)$ can be calculated from the current error $\epsilon(k)$:

$$\epsilon(k) = s(k) - y(k) \quad (10)$$

and $\epsilon(k+i)$, which is the error found i sampling instants later

$$\epsilon(k+i) = \mathrm{e}^{-iT_s/T_{ref}}\epsilon(k) = \lambda^i\epsilon(k), \quad (11)$$

where T_s is the sampling interval and $\lambda = \mathrm{e}^{-T_s/T_{ref}} \in (0, 1)$.

A suitable formulation for the reference trajectory is

$$r(k+i|k) = s(k+i) - \epsilon(k+i) = s(k+i) - \mathrm{e}^{-iT_s/T_{ref}}\epsilon(k), \quad (12)$$

where $r(k+i|k)$ is the reference trajectory at time $k+i$ evaluated in k. The availability of an internal prediction

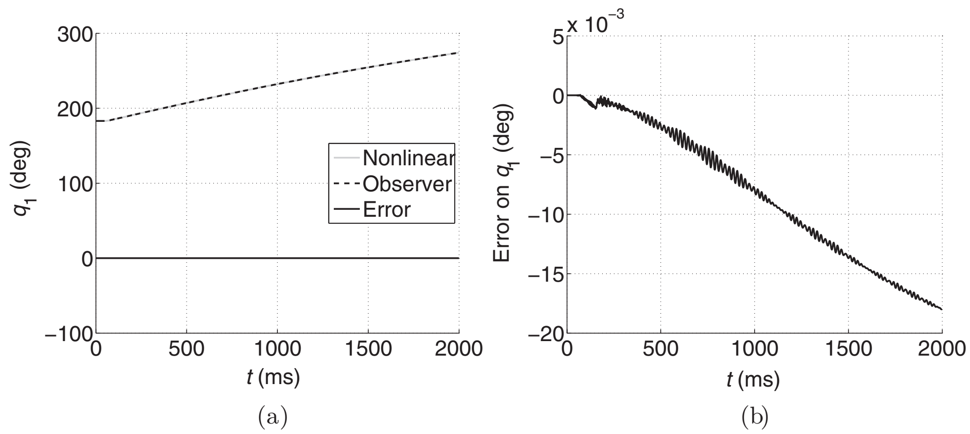

Fig. 3. (a) Comparison of actual and estimated angular position, estimation error for q_1; (b) absolute error on q_1.

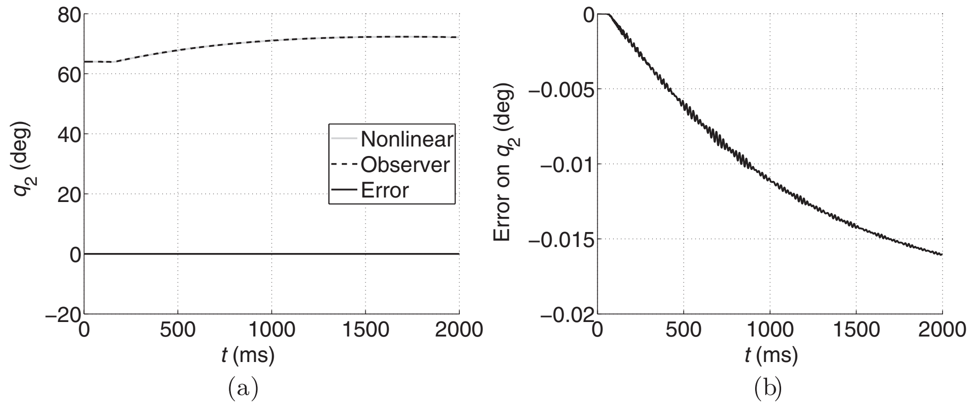

Fig. 4. (a) Comparison of actual and estimated angular position, estimation error for q_2; (b) absolute error on q_2.

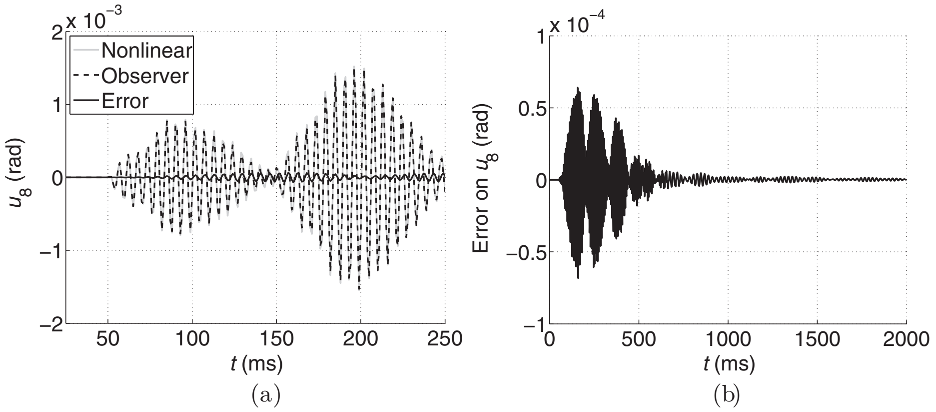

Fig. 5. (a) Comparison of actual and estimated nodal displacement, estimation error for u_8; (b) absolute error on u_8.

model allows to compute an estimation of the future input sequence $\hat{w}(k+i|k)$ with $i = 0, 1, \ldots, H_p - 1$. H_p is the *prediction horizon*, i.e., the length measured as number of discrete time steps over which an estimation of the plant future dynamics is calculated.

The control variable sequence $\{\hat{w}(k|k), \hat{w}(k+1|k), \ldots, \hat{w}(k+H_c+1|k)\}$ is calculated by minimizing a cost function. This sequence is composed by H_c steps. The length H_c is called control horizon, and usually $H_c < H_p$. After computing the future control sequence, only the first element of this sequence is applied as the input signal to the plant: $w(k) = \hat{w}(k|k)$. At the following sampling interval the sequence of output measurements, predictions and input trajectory calculation is repeated, yielding $y(k+1)$, $r(k+i+1|k+1)$ with $i = 0, 1, \ldots, H_p - 1$. The prediction is formulated over $k+1+i$, where $i = 0, 1, \ldots, H_p - 1$. From those, a new sequence of input values can be calculated: $w(k+1+i) = \hat{w}(k+1+i|k+1)$ with $i = 0, 1, \ldots, H_p - 1$. Again, only the first element of the reference trajectory is applied to the plant: $w(k+1) = \hat{w}(k+1|k+1)$ and so on. Since the length of the prediction horizon H_p remains constant over the time, and the prediction horizon "slides" forward each time step, this strategy is commonly mentioned as receding horizon strategy. A graphical representation of this concept can be found in Fig. 6.

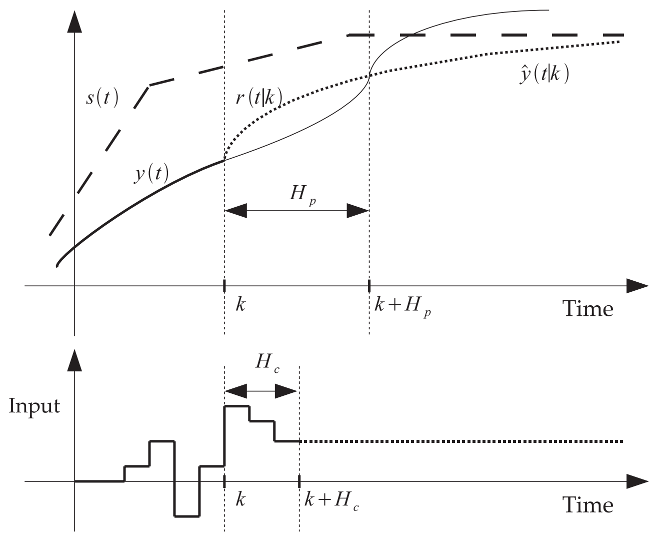

Fig. 6. Receding horizon strategy.

4.2. *Model prediction*

Given a LTI plant in state-space form

$$\begin{cases} \mathbf{x}(k+1) = \mathbf{F}\mathbf{x}(k) + \mathbf{G}\mathbf{w}(k) \\ \mathbf{y}(k) = \mathbf{H}\mathbf{x}(k) \\ \mathbf{z}(k) = \mathbf{H}_z\mathbf{x}(k), \end{cases} \tag{13}$$

where $\mathbf{x}(k)$ is the state vector, while $\mathbf{y}(k)$, $\mathbf{z}(k)$, and $\mathbf{w}(k)$ are the vectors of outputs, controlled variables, and inputs, respectively. $\mathbf{F}$,$\mathbf{G}$, $\mathbf{H}$, and $\mathbf{H}_z$ are the discrete time version of the matrices of LTI linearized model presented in Section 3.1. Assuming that the whole state $\mathbf{x}(k)$ is measured, the future behavior of the plant at time k over H_p steps, $[\hat{\mathbf{x}}(k+1|k), \ldots, \hat{\mathbf{x}}(k+H_p|k)]$, can be evaluated by iterating the first of Eq. (13)

$$\begin{aligned}
&\hat{\mathbf{x}}(k+1|k) = \mathbf{F}\mathbf{x}(k) + \mathbf{G}\hat{\mathbf{w}}(k|k)\\
&\hat{\mathbf{x}}(k+2|k) = \mathbf{F}\hat{\mathbf{x}}(k+1|k) + \mathbf{G}\hat{\mathbf{w}}(k+1|k)\\
&\vdots\\
&\hat{\mathbf{x}}(k+H_p|k) = \mathbf{F}\hat{\mathbf{x}}(k+H_p-1|k) + \mathbf{G}\hat{\mathbf{w}}(k+H_p-1|k)\\
&= \mathbf{F}^{H_p}\mathbf{x}(k) + \mathbf{F}^{H_p-1}\mathbf{G}\hat{\mathbf{w}}(k|k) + \cdots + \mathbf{G}\hat{\mathbf{w}}(k+H_p-1|k).
\end{aligned} \tag{14}$$

Such equation can be written as

$$\begin{bmatrix} \hat{\mathbf{x}}(k+1|k) \\ \vdots \\ \hat{\mathbf{x}}(k+H_c|k) \\ \hat{\mathbf{x}}(k+H_c+1|k) \\ \vdots \\ \hat{\mathbf{x}}(k+H_p|k) \end{bmatrix} = \underbrace{\begin{bmatrix} \mathbf{F} \\ \vdots \\ \mathbf{F}^{H_c} \\ \mathbf{F}^{H_c+1} \\ \vdots \\ \mathbf{F}^{H_p} \end{bmatrix} \mathbf{x}(k) + \begin{bmatrix} \mathbf{G} \\ \vdots \\ \sum_{i=0}^{H_c-1} \mathbf{F}^i\mathbf{G} \\ \sum_{i=0}^{H_c} \mathbf{F}^i\mathbf{G} \\ \vdots \\ \sum_{i=0}^{H_p-1} \mathbf{F}^i\mathbf{G} \end{bmatrix} \mathbf{w}(k+1)}_{past}$$

$$+ \underbrace{\begin{bmatrix} \mathbf{G} & \cdots & 0 \\ \mathbf{F}\mathbf{G}+\mathbf{G} & \cdots & 0 \\ \vdots & \ddots & \vdots \\ \sum_{i=0}^{H_c-1} \mathbf{F}^i\mathbf{G} & \cdots & \mathbf{G} \\ \sum_{i=0}^{H_c} \mathbf{F}^i\mathbf{G} & \cdots & \mathbf{F}\mathbf{G}+\mathbf{G} \\ \vdots & \vdots & \vdots \\ \sum_{i=0}^{H_p-1} \mathbf{F}^i\mathbf{G} & \cdots & \sum_{i=0}^{H_p-H_c} \mathbf{F}^i\mathbf{G} \end{bmatrix} \begin{bmatrix} \Delta\hat{\mathbf{w}}(k|k) \\ \vdots \\ \Delta\hat{\mathbf{w}}(k+H_c-1|k) \end{bmatrix}}_{future} \tag{15}$$

or, in a compact form

$$\mathcal{X}(k) = \mathcal{F}\mathbf{x}(k) + \mathcal{G}\mathbf{w}(k+1) + \Xi\Delta\mathcal{W}(k). \tag{16}$$

Prediction values of outputs and controlled variables are calculated from the predicted states by

$$\begin{bmatrix} \hat{\mathbf{y}}(k+1|k) \\ \vdots \\ \hat{\mathbf{y}}(k+H_p|k) \end{bmatrix} = \begin{bmatrix} \mathbf{H} & 0 & \cdots & 0 \\ 0 & \mathbf{H} & \cdots & 0 \\ \vdots & \vdots & \ddots & \vdots \\ 0 & 0 & \cdots & \mathbf{H} \end{bmatrix} \begin{bmatrix} \hat{\mathbf{x}}(k+1|k) \\ \vdots \\ \hat{\mathbf{x}}(k+H_p|k) \end{bmatrix} \tag{17}$$

$$\begin{bmatrix} \hat{\mathbf{z}}(k+1|k) \\ \vdots \\ \hat{\mathbf{z}}(k+H_p|k) \end{bmatrix} = \begin{bmatrix} \mathbf{H}_z & 0 & \cdots & 0 \\ 0 & \mathbf{H}_z & \cdots & 0 \\ \vdots & \vdots & \ddots & \vdots \\ 0 & 0 & \cdots & \mathbf{H}_z \end{bmatrix} \begin{bmatrix} \hat{\mathbf{x}}(k+1|k) \\ \vdots \\ \hat{\mathbf{x}}(k+H_p|k) \end{bmatrix} \tag{18}$$

or, in a compact form

$$\mathcal{Y}(k) = \mathcal{H}_y\mathcal{X}(k) \tag{19}$$

$$\mathcal{Z}(k) = \mathcal{H}_z\mathcal{X}(k) = \Psi\hat{\mathbf{x}}(k) + \Upsilon\mathbf{w}(k-1) + \boldsymbol{\Theta}\Delta\mathcal{W}(k), \tag{20}$$

where: $\Psi = \mathcal{H}_z\mathcal{F}$, $\Upsilon = \mathcal{H}_z\mathcal{G}$, $\boldsymbol{\Theta} = \mathcal{H}_z\Xi$.

4.3. *Constrained optimization solution*

As already stated before, the evaluation of the optimal control sequence is obtained by minimizing a cost function. According to the receding horizon principle, such evaluation is performed at every iteration of the controller, and only the first element of the computed control sequence $\mathcal{W}(\|)$ is actually fed to the plant. $\mathcal{W}(k)$ is calculated as the minimum of the cost function

$$\mathcal{V}(k) = \sum_{i=1}^{H_p} \|\hat{z}(k+i|k) - r(k+i)\|_Q^2 + \sum_{i=0}^{H_c-1} \|\Delta\hat{w}(k+i|k)\|_R^2\,, \tag{21}$$

which can also be written as

$$\mathcal{V}(k) = \|\mathcal{Z}(k) - \mathcal{T}(k)\|_Q^2 + \|\Delta\mathcal{W}(k)\|_R^2\,. \tag{22}$$

$\mathbf{Q}$ and $\mathbf{R}$ are diagonal matrices of weights: the former is used to penalize the quadratic norm of the deviation of the output from the desired trajectory, while the latter penalizes the magnitude and the change-rate of the control variable. The minimization of the cost function $\mathcal{V}(k)$ can be constrained. In this case, linear inequalities on the control variables, their change rate, and the controlled outputs are considered as

$$w_{i\,\min} \le w_i(k) \le w_{i\,\max}, \tag{23}$$

$$\Delta w_{i\,\min} \le \Delta w_i(k) \le \Delta w_{i\,\max}, \tag{24}$$

$$z_{i\,\min} \le z_i(k) \le z_{i\,\max.} \tag{25}$$

All the inequalities can be merged into a single matricial inequality, using Eqs. (16), (19), and (20), as functions of the vector of increments of the control variables $\Delta\mathcal{W}(k)$:

$$\boldsymbol{\Theta}\Delta\mathcal{W}(k) \le \boldsymbol{\theta}. \tag{26}$$

The procedure followed to rearrange the inequalities is omitted, the details can be found in ref. [26]. Therefore, the minimization problem can be stated as

$$\begin{cases} \min\limits_{\Delta\mathcal{W}(k)} \mathcal{V}(k) \\ s.t. \quad \Theta\Delta\mathcal{W}(k) \le \vartheta \end{cases} \tag{27}$$

with

$$\mathcal{V}(k) = \|\mathcal{Z}(k) - \mathcal{T}(k)\|_Q^2 + \|\Delta\mathcal{W}(k)\|_R^2 .$$

It can be shown (see ref. [26]) that the minimization problem (27) is equivalent to

$$\begin{cases} \min\limits_{\Delta\mathcal{W}(k)} \Delta\mathcal{W}(k)^{\mathrm{T}}\mathcal{H}\Delta\mathcal{W}(k) - \mathcal{G}^{\mathrm{T}}\Delta\mathcal{W}(k) \\ \qquad s.t. \quad \Theta\Delta\mathcal{W}(k) \le \vartheta \end{cases} \tag{28}$$

since $\mathcal{V} = \text{constant} - \Delta\mathcal{W}(k)^{\mathrm{T}}\mathcal{G} + \Delta W(k)^{\mathrm{T}}\mathcal{H}\Delta\mathcal{U}(k)$, where $\mathcal{G} = 2\mathbf{\Theta}^{\mathrm{T}}Q\mathcal{E}(k)$, $\mathcal{H} = \mathbf{\Theta}^{\mathrm{T}}Q\mathbf{\Theta} + R$. $\mathcal{E}(k)$ is the future evolution of tracking error from time k to $k + H_p$, i.e., $\mathcal{E}(k) = \mathcal{Z}(k) - \mathcal{T}(k)$ evaluated at time k.

This minimization problem is a quadratic programming problem since it is in the form: $\min_\theta \frac{1}{2}\theta^{\mathrm{T}}\Phi\theta + \phi^{\mathrm{T}}\theta$ with $\Omega\theta \le \omega$. Moreover, this problem is convex, see ref. [26], i.e., the local minimum is also the global minimum. Therefore, the optimal control sequence $\Delta\mathcal{W}(k)$ over the control horizon H_c can be calculated by setting to zero the gradient of $\mathcal{V}(k)$:

$$\Delta\mathcal{W}(k)_{opt} = \frac{1}{2}\mathcal{H}^{-1}\mathcal{G}. \tag{29}$$

5. MPC Control: Numerical Results of Trajectory Tracking in the Joints Space

In this section, the effectiveness of the proposed control strategy for simultaneous path following and vibration reduction will be demonstrated and discussed. This evaluation is conducted trough extensive simulation, using the MATLAB/Simulink environment. The effectiveness of the MPC controller as a regulator has already been proven in refs. [21, 22], but here, the focus moves from regulation problem to tracking problem. Moreover, it should be pointed out that the problem of position control in a multi-DOFs system is nontrivial since a lack of synchronization between the motion of the axis leads to severe worsening to the accuracy. For this reason, a reference lookahead strategy has been included in the predictive control, and the effective improvement is shown. Effects of different choices for some of the tuning parameters of the controller, namely, the two horizons H_p and H_c, are investigated in terms of accuracy of reference tracking and vibration damping by the means of extensive sets of simulations. A list of the tuning parameters of the implemented control can be found in Table III, while the block diagram of the closed-loop control used for the simulation is reported in Fig. 7.

Table III. MPC tuning parameters.

Symbol	Description
H_p	prediction horizon
H_c	control horizon
T_s	sampling time
$w_{\tau 1}, w_{\tau 2}$	weights on torques
$w_{\delta\tau 1}, w_{\delta\tau 2}$	weights on the change rate of torques
$w_{u_1}, w_{u_{18}}$	weights on nodal displacements
w_{q_1}, w_{q_2}	weights on angular position of the cranks

The capabilities of the MPC controller both in terms of position tracking and vibration control have been tested using two constant speed trajectories for q_1 and q_2. In these tests, the mechanism performs two high-speed rotation of the first and the fourth link: q_1 rotates 45°, while q_2 rotates 30° in 500 ms. As it can be seen in Fig. 8, the closed-loop system exhibits optimal performances: the reference tracking is very good and has almost no delay. The torques provided by the two actuators are displayed in Fig. 9. In Fig. 8, it can be seen that the closed-loop system damps very efficiently the vibration that arises in the mechanism when the two angular positions q_1 and q_2 have discontinuous velocities and accelerations.

5.1. *Effects of the reference lookahead and control tuning*

The promptness in reference tracking exhibited in Fig. 8 is heavily influenced by the reference lookahead system used by the MPC controller. As already stated in Eq. (18), the optimal control sequence is calculated at every iteration in order to minimize (also) the quadratic norm $\|\mathcal{Z}(k) - \mathcal{T}(K)\|$. Such a value is the quadratic norm of the tracking error $\mathcal{E}(k) = \mathcal{Z}(k) - \mathcal{T}(K)$ in which $\mathcal{Z}(k)$ and $\mathcal{T}(k)$ are the evolution of controlled outputs and the reference from actual time k to $k + H_p$.

When reference lookahead is not implemented, the future reference values are estimated simply by $r(k+i) = r(k)\ \forall i \in [1, H_p - 1]$, so $\mathcal{T}(k) = r(k)$, which is the exact prediction only for constant or step-changing reference signals. The enhancing in terms of reference tracking obtainable with reference lookahead can be seen in Fig. 10: the same test presented in Fig. 8 is here compared with the results obtained without reference lookahead. It can be seen that the adoption of a lookahead strategy reduces the delay of the response. This effect is even more evident when the change rate of the reference trajectory and the prediction horizon are increased.

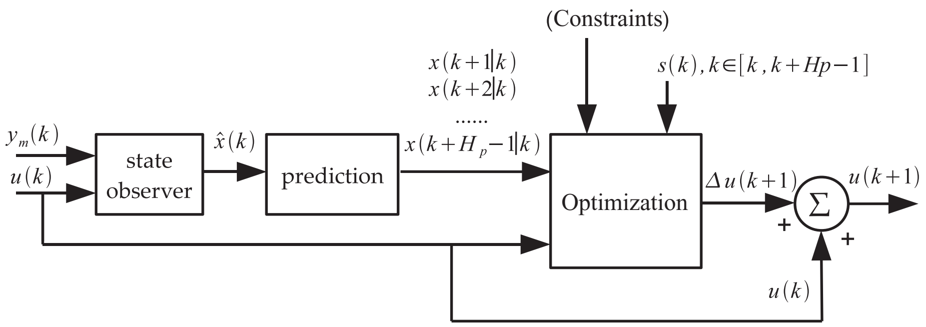

Fig. 7. Structure of the MPC controller.

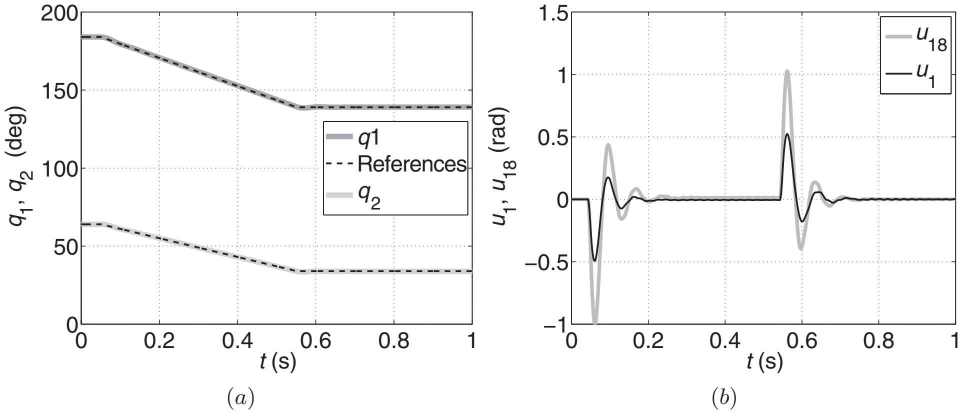

Fig. 8. Closed-loop performances: (a) evolution of angular positions q_1 and q_2; (b) angular displacements u_1 and u_{18} for reference tracking in the operational space.

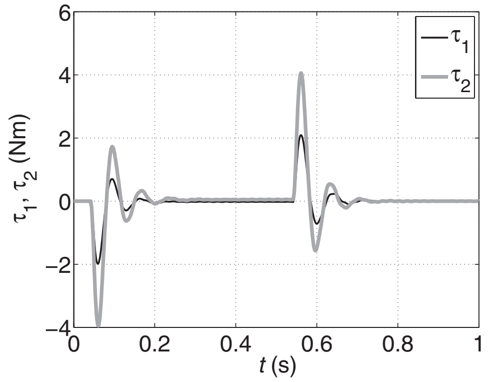

Fig. 9. Closed-loop performances: torques τ_1 and τ_2 applied by the two actuators.

The tuning of the MPC controller is also influenced by the values of the weights used in the minimization problem (see Eq. 17) as the diagonal entries of matrices $\mathbf{Q}$ and $\mathbf{R}$. These weights are:

- w_{τ_1} and w_{τ_2}: weights on the two torques applied to the first and the fourth link, respectively.
- $w_{\delta\tau_1}$ and $w_{\delta\tau_2}$: weights on the change rate of the two torques applied to the first and the fourth link, respectively.
- w_{u_1}, $w_{u_{18}}$: weights on the two controlled nodal displacements u_1 and u_{18}, respectively.
- w_{q_1}, w_{q_2}: weights on the angular positions q_1 and q_2, respectively.

Then, the behavior of the controller depends also on the length of the two horizons: the prediction horizon H_p

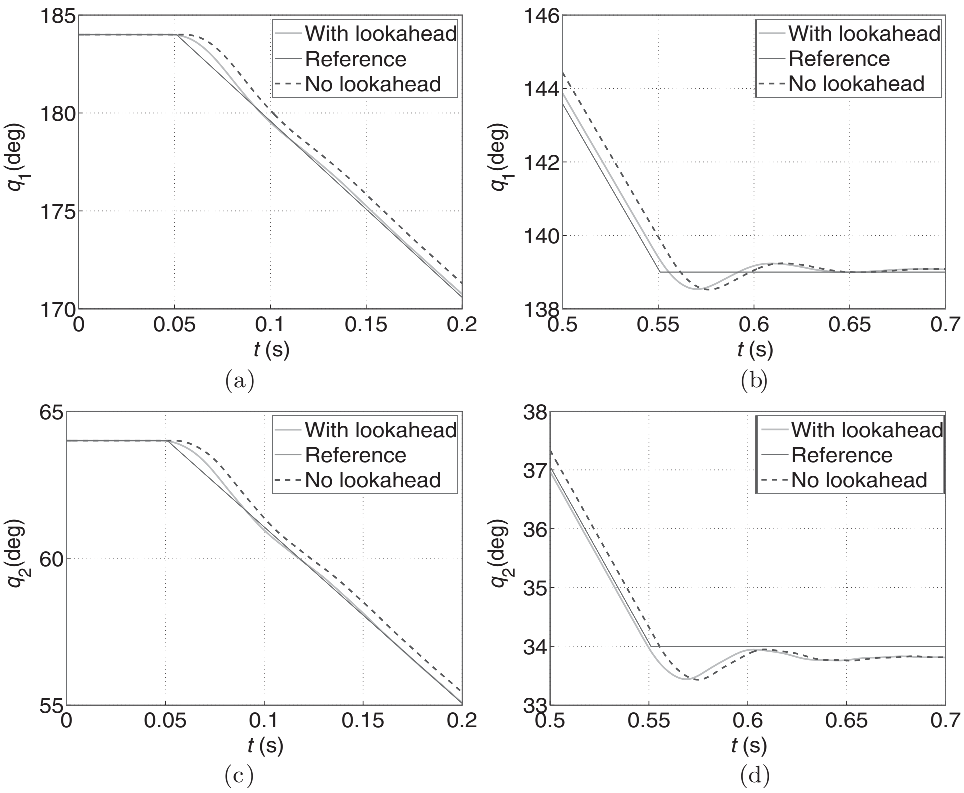

Fig. 10. Comparison of reference tracking with and without reference lookahead: (a) and (b) angular position q_1; (c) and (d) angular position q_2.

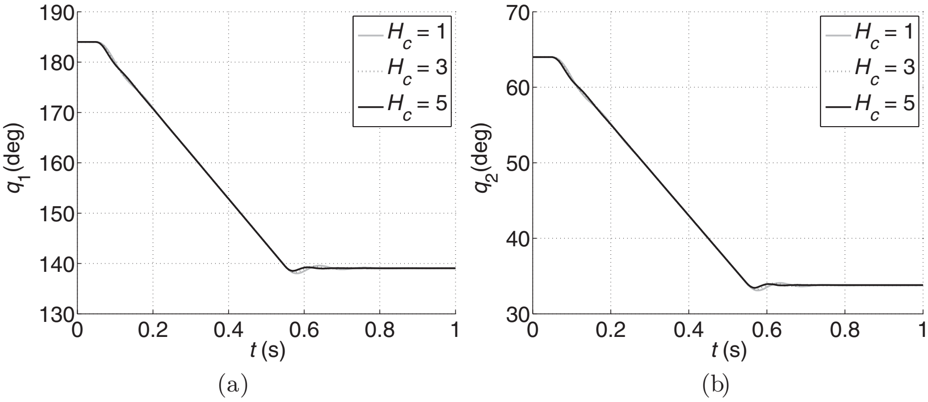

Fig. 11. Effects of different values of the control horizon H_c ($H_p = 10$): (a) angular position q_1 of the first link; (b) angular position q_2 of the fourth link.

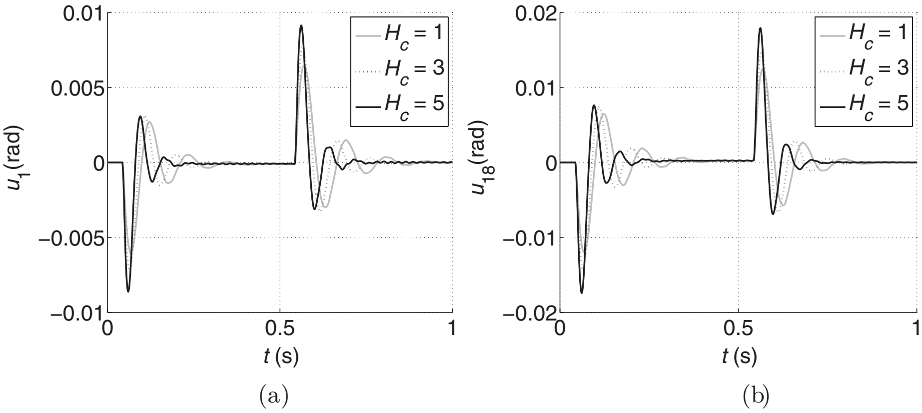

Fig. 12. Effects of different values of the control horizon H_c ($H_p = 10$): (a) angular displacement u_1 along the first link; (b) angular displacement u_{18} along the fourth link.

and the control horizon H_c. For all the tests conducted, the sampling frequency is $T_s = 1$ ms. The tuning for the test shown in Figs. 8–10 is as follows: $w_{\tau_1} = w_{\tau_2} = w_{\delta\tau_1} = w_{\delta\tau_2} = 0.1$; $w_{u_1} = 3000$, $w_{u_{18}} = 2000$, $w_{q_1} = 4000$, $w_{q_2} = 7000$, $H_p = 10$, $H_c = 5$. It can be noticed in Fig. 10(d) that the position tracking for q_2 (with and without lookahead) is less effective than the tracking of q_1. This is caused by the choice of the linearization point. In this case, q_2 is more sensitive than q_1 to this approximation since the sensibility coefficients for q_2 are less linear than those of q_1 along the considered trajectory. The same behavior can be shown for q_1 if the trajectories of the two joints are swapped.

5.2. *Influence of the control horizon H_c on closed-loop performance*

In order to show how the choice of the control horizon and the prediction horizon affects the closed-loop response, extensive sets of simulations have been conducted. A few results are displayed in Figs. 11 and 12 in which the effects of altering only the length of the control horizon are reported. From Fig. 11, it can be seen that altering the control horizon has a limited effect on the reference tracking of the two angular positions q_1 and q_2: with lower values of H_c, the angular movement appears to be slightly less accurate. The parameter H_c influences mainly the readiness of the system in terms of vibration reduction: as can be inferred from Fig. 12, the choice of higher values of the control horizon leads to higher vibration peak but with a more fast damping. This effect can be thought as a higher gain of the controller. Results are shown with H_c up to 5 since further increase does lead to little or no improvements.

5.3. *Influence of the prediction horizon H_p on closed-loop performance*

In Figs. 13 and 14, the effects of altering the prediction horizon H_p are shown. From those graphs, it can be inferred that H_p influences mainly the damping performances of the closed-loop system. From Fig. 13, the vibration of u_1 and u_{18} requires more time to be damped when choosing shorter H_p. At the same time, the reference tracking of q_1 and q_2 is more accurate when H_p is higher. Here, the results are shown with H_p up to 20 since it has been proven that the performance enhancing is very slight when going beyond this threshold.

The previous observations can be summarized by the graphs in Fig. 15, which report the results of several simulations obtained by changing the values of the prediction and control horizons. The tuning parameters of the MPC control have been chosen as in Table IV. A large number of tests have been conducted by performing the same tests whose results are displayed in Figs. 10 and 11, but here, the prediction horizon ranges from 3 to 20, and the control horizon ranges from 1 to H_p since it makes no sense to set $H_p > H_c$. All the values of the other parameters of the controller are kept the same as the previous simulations.

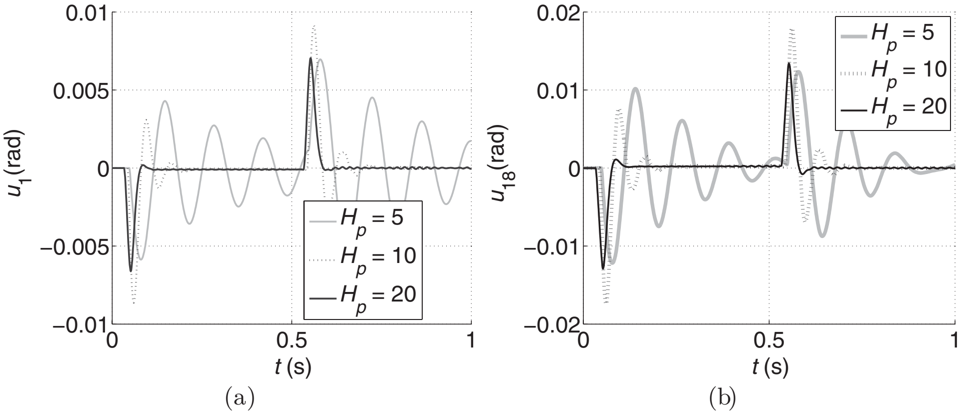

Fig. 13. Effects of different values of the prediction horizon H_p ($H_c = 5$): (a) angular displacement u_1; (b) angular displacement u_{18}.

For sake of simplicity, two indices have been defined, as follows:

$$k_1 = \|\Delta \mathbf{q}(t)\|_\infty$$
$$k_2 = \|\Delta \mathbf{q}(t)\|_\infty \quad \text{with} \quad t \in [0.9\,\text{s}, 1\,\text{s}] \tag{30}$$

being $\Delta\mathbf{q}(t)$ the tracking error, i.e., $\Delta\mathbf{q}(t) = \left\|\mathbf{q}_D(t) - \mathbf{q}(t)\right\|$ in which $\mathbf{q}_D(t) = [q_{1D}(t), q_{2D}(t)]$ and $\mathbf{q}(t) = [q_1(t), q_2(t)]$ are the desired and actual angular positions of the cranks, respectively. The index k_1 describes the infinity norm of the quadratic error. Namely, it measures the error (evaluated in the joint space) between the desired and the actual position of the controlled cranks, while the index k_2 is defined as the infinity norm of the tracking error at the end of the test. Therefore, it is closely related to the steady-state error. As it can be inferred by comparing the two graphs, the value of H_p affects in different ways the mentioned indices.

In Fig. 15(a), it can be seen that the maximum path error can be minimized by choosing $H_p = 14$ and $H_c > 4$. It can also be noticed that the maximum tracking error is highly sensitive to the prediction horizon, as long as the ratio between H_c and H_p is sufficiently high. In Fig. 15(b), the value of performance index k_2 is plotted versus H_p and H_c: it can be seen that, in order to reduce the steady-state error,

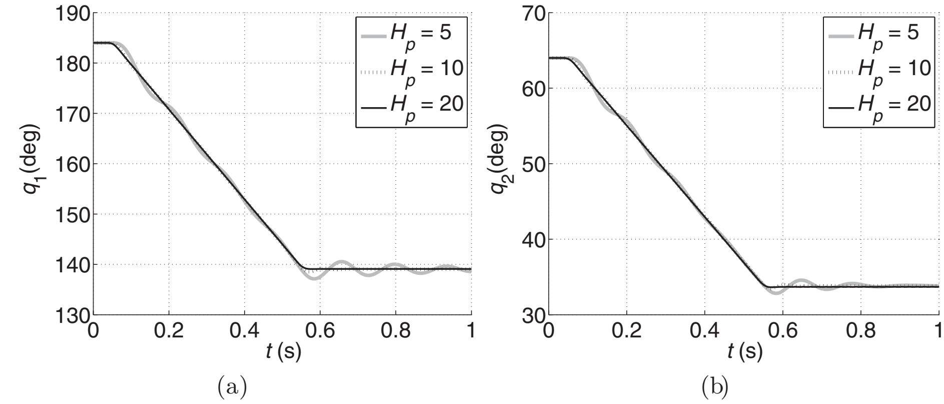

Fig. 14. Effects of different values of the prediction horizon H_p ($H_c = 5$): (a) angular position q_1 of the first link; (b) angular position q_2 of the fourth link.

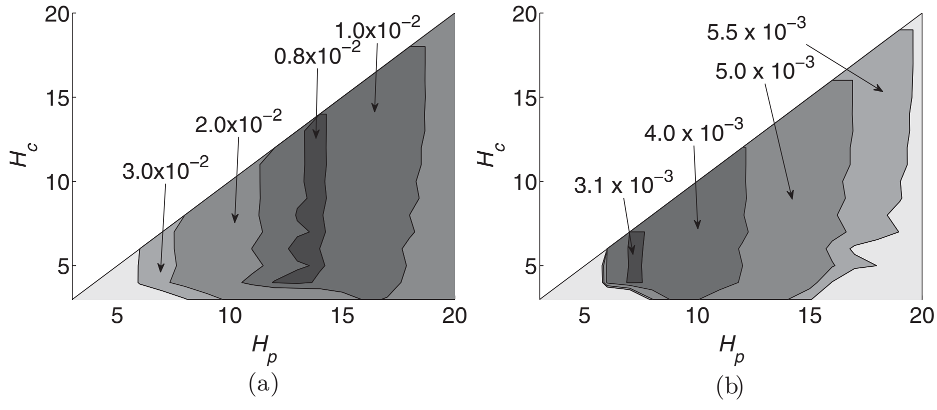

Fig. 15. Effects of different values of H_p and H_c: (a) performance index k_1; (b) performance index k_2.

Table IV. Values of MPC tuning parameters.

Parameters	Value
H_p	1–20
H_c	1 - Hp
T_s	1 kHz
$w_{\tau 1}$, $w_{\tau 2}$	0.1
$w_{\delta\tau 1}$, $w_{\delta\tau 2}$	0.1
w_{u_1}	3000
$w_{u_{18}}$	2000
w_{q_1}	4000
w_{q_2}	7000

H_p should be chosen to be 7. Again, H_c has less influence than H_p on the performances of the closed-loop system when position accuracy is the main concern.

5.4. Evaluation of robustness

Exhaustive numerical tests have been conduced to test the robustness of the controller to mismatches between the plant and its model used for prediction and observation. This approach to robustness evaluation has been employed in other papers.[18,22] Simulation results show that the MPC controller can withstand severe plant-model parametric mismatches. In Fig. 16, the response of the nominal plant is compared to the response of two different mismatched plants. In the perturbed plant, some fundamental parameters have been changed, such as the elastic modulus E and the linear mass density m of the links. Moreover, two uncorrelated noise signals have been added to the torques. These two noisy disturbance act as severe unmeasured noises since the state observer cannot measure them. The simulation results plotted in Fig. (16) refer to (1) plant with E and m reduced by 20%, uncorrelated torque noise with PSD = 1 $\times 10^{-4}$; (2) plant with E and m increased by 20%, uncorrelated torque noises with PSD = 1 $\times 10^{-4}$; and (3) nominal plant.

The MPC controller shows a robust behavior: even when noise is added, the response of the system has just a small degradation of the performances, nevertheless the stability as been preserved. The response in terms of angular position tracking is not shown, since the difference in performance from the nominal case is practically unnoticeable. As it is evident in Fig. 16, the increased level of vibration is caused solely by the torque disturbances since the reference tracking of q_1 and q_2 has an almost undetectable degradation, and the closed-loop system retains its stability. It should be pointed out that the magnitudes of both the additive noises and the parametric mismatches artificially added to the closed-loop system are far beyond the unavoidable mismatches that arise in typical experimental tests.

6. Numerical Investigation of End-Effector Trajectory Tracking

In the previous sections, the effectiveness of the proposed control strategy has been proved for tasks defined in the joint space. Nevertheless, the manipulator tasks are defined, in general, in the operational space. In such a space, the control requirements become much stricter, since small and negligible errors in joint position could cause large errors in the end-effector position, owing to the kinematic structure of the manipulator. In this section, a suitable test bench will be carried out to prove the effectiveness of the proposed control approach for a task defined in the operational space, as well. The end effector (assumed to be fixed to the joint C) should move from the position C_0 (-100 mm, 460 mm) toward position C_f (400 mm, 460 mm) following the straight line that passes between the mentioned points (Fig. 17). The movement must be executed in $T = 1$ s and the vibrations as well as the position errors should be kept as small as possible.

The trajectory in the Cartesian space has been planned by using a third degree polynomial function, whose coefficients have been set by the constraints on the final and initial positions and the related velocities (forced to zero). Figure 18 shows the resultant joints position, velocity, and acceleration obtained through the inverse kinematic algorithm. It can be observed that the desired motion of each controlled joint is wider than 80°. Therefore, the task looks to be heavy since the movement has to be completed very quickly ($T = 1$ s). In Fig. 19, four surfaces show the sensibility coefficients w_{ij} end-effector C of the ERLS as a function of the rigid coordinate's values q_1 and q_2, defined by the following equation:

$$\dot{\mathbf{C}} = \mathbf{S}_C(\mathbf{q})\dot{\mathbf{q}} = \begin{bmatrix} w_{11} & w_{12} \\ w_{21} & w_{22} \end{bmatrix}_{(q_1,q_2)} \begin{bmatrix} \dot{q}_1 \\ \dot{q}_2 \end{bmatrix}. \tag{31}$$

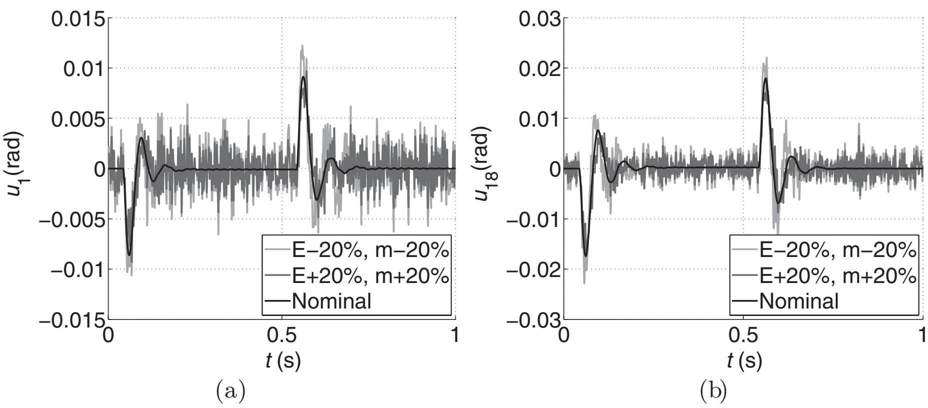

Fig. 16. Comparison of the response of the nominal and two perturbed plants with added noise: (a) angular displacement u_1; (b) angular displacement u_{18}.

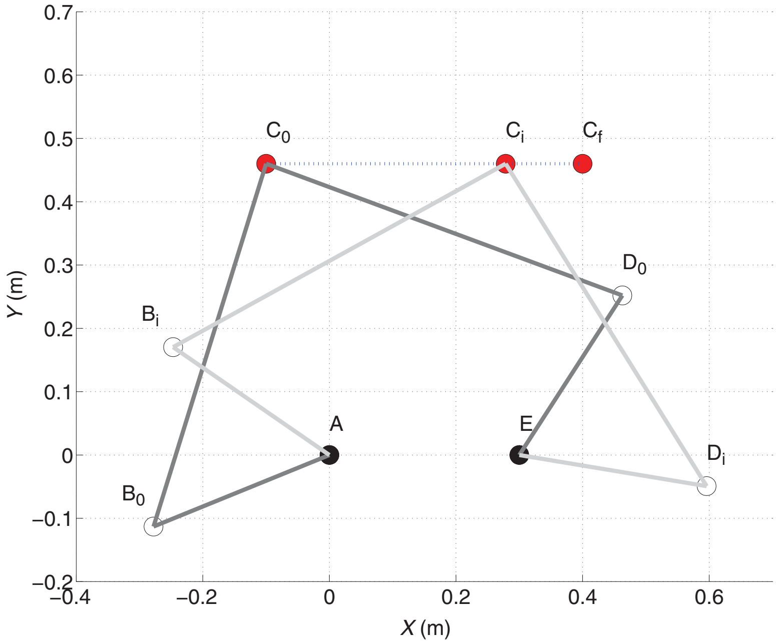

Fig. 17. (Colour Online) Reference trajectory for the end effector in the operational space.

The sensibility coefficients are used to evaluate the speed of a generic point belonging to the manipulator form from the speed of the free coordinates. The curves in black in Fig. 19 show the w_{ij} values corresponding along the planned trajectory. It can be seen that for the chosen trajectory the sensibility coefficients vary rather slowly. This behavior helps the effectiveness of the assumed linear observer, even if the mechanism moves far away from the linearization configuration.

Figure 18 proves the efficiency of suggested control approach, by displaying the real versus planed trajectories, while Fig. 20 shows the related u_1 and u_{18} nodal

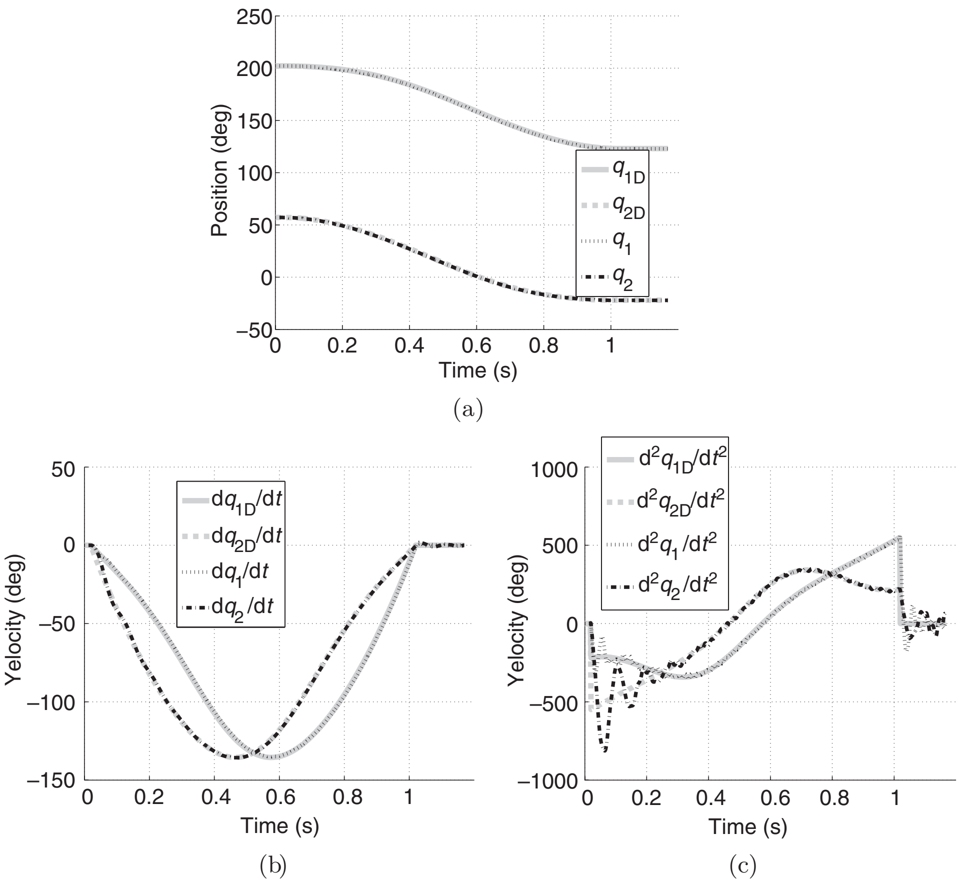

Fig. 18. Actual q_i and planned q_{iD} trajectories: (a) positions, (b) velocities, and (c) acceleration.

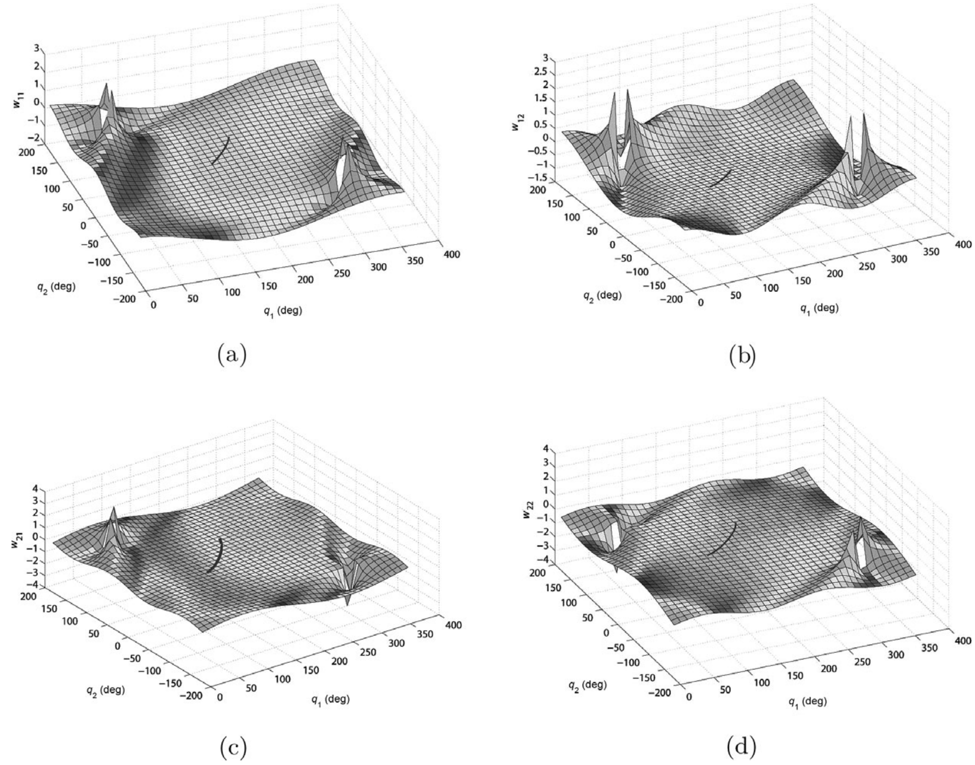

Fig. 19. Evolution of sensitivity coefficients for the end effector position along the planned trajectories: (a) w_{11}; (b) w_{12}; (c) w_{21}; (d) w_{22}.

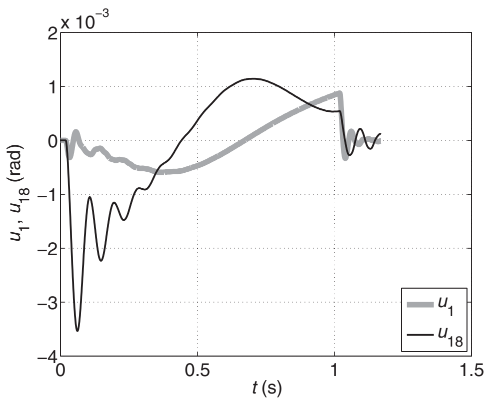

Fig. 20. Nodal displacements u_1 and u_{18}.

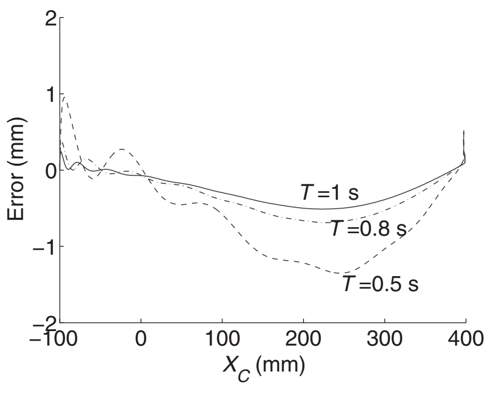

Fig. 21. Path following error of the manipulator end-effector C along the desired trajectory with different task execution times.

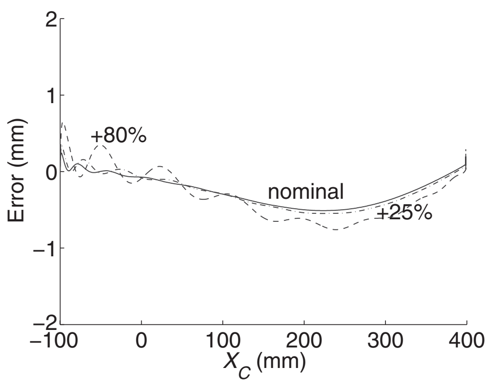

Fig. 22. Effects on the trajectory error of increments on deformation weights.

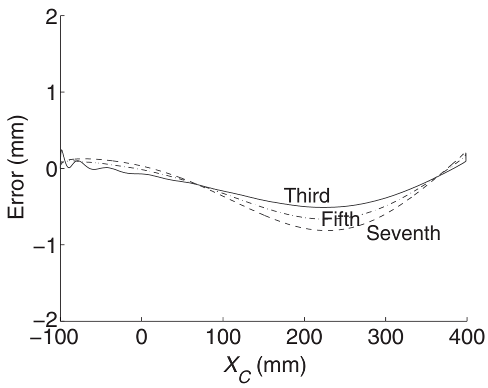

Fig. 23. Effects of the interpolating function on the trajectory error.

displacements and proves the MPC effectiveness in keeping small the manipulator vibration. It can be shown that both position and velocity trajectories are followed quite accurately, while some discrepancies appear as far as the acceleration signals are concerned. Figure 21 shows the end-effector tracking error that the manipulator makes while

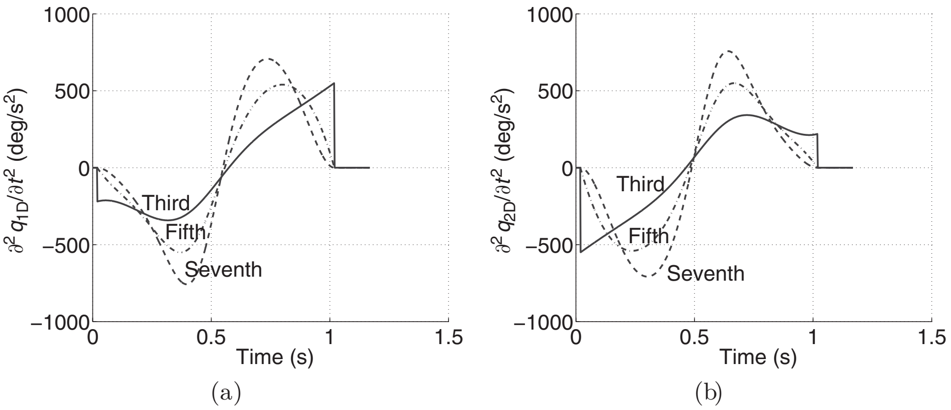

Fig. 24. (a) Velocities and (b) acceleration of q_1 and q_2 with third-, fifth-, and seventh-order interpolation functions.

following the trajectory. It can be shown that the latter is always less than 0.6 mm for $T = 1$ s. It increases up to the middle region of the desired trajectory and decreases toward the final position. This behavior can be easily explained if the controller behavior, which tends to slow down any velocity change, so as to reduce the vibration amplitude, is considered. Therefore, the MPC smooths the trajectories and delays the trajectory following.

The controller effects on vibration minimization become more comprehensible by looking at Figs. 21 and 22. Figure 21 displays the tracking error when the task is executed in a shorter time. Since, in this case, changes in velocity and acceleration are greater than in the previous simulation, the MPC controller delays much more the path following. On the other hand, Fig. 22 shows what happens if the MPC weights on the vibration amplitude are changed. It can be seen that by augmenting the weights on the deformations, a clear degrading effect occurs on the end-effector accuracy. Therefore, much attention must be paid in selecting the MPC weights: the behavior of the overall mechanism strongly depends on their values and a suitable trade-off between the requirements on trajectory error and vibration reduction must be found.

Figure 23 shows the effects of different choices on the interpolating function. It is well known that for a compliant mechanism, discontinuities on the reference trajectory should be limited to derivatives of the highest order and, in any case, these should be kept as small as possible. Figure 24 seems to contradict this guideline: increasing the interpolating function order (therefore, reducing the discontinuities to the highest order derivatives) decreases the controller performances. This behavior might be interpreted by considering that any increment of the interpolating function order increases the maximum values of the velocities and acceleration increase as well. Therefore, it requires a heavier controller action, which raises the delay on the path following.

7. Conclusions

This paper has presented an investigation of a model predictive control system for a flexible-link mechanisms with multiple actuators. The aim of the presented solution is to control both the position and the elastic displacement of the plant. The design of the controller is based on a very accurate linearized dynamic model. The performance in terms of trajectory tracking is evaluated for tasks defined both in the joints space and the operational space. The effects of choosing different trajectory planning algorithms for point-to-point motion in the operational space are investigated as well. It has been proved that the control system is very effective in both trajectory tracking and vibration suppression even in high-speed and extensive movement range task, and it is robust to both parametric mismatches between the actual and the modeled plant and to unmeasured input disturbances. The experimental tests are currently under development. The authors are working on a real-time implementation of the control system shown in this paper. Results will be available as soon as the problem caused by the hardware of choice will be solved.

References

1. A. R. Fraser and R. W. Daniel, *Perturbation Techniques for Flexible Manipulators* (Kluwer Academic Publisher, Norwell, MA, USA, 1991).
2. S. K. Dwivedy and P. Eberhard, "Dynamic analysis of flexible manipulators, a literature review," *Mech. Mach. Theory* **41**, 749–777 (2006).
3. S. Nagarajan and D. A. Turcic, "Lagrangian formulation of the equation of motion for elastic mechanisms with mutual dependence between rigid body and elastic motions. Part II: Systems equations," *ASME J. Dyn. Sist. Meas. Control* **112**, 203–214 (1990).
4. M. Giovagnoni, "A numerical and experimental analysis of a chain of flexible bodies," *J. Dyn. Syst. Meas. Control* **113**, 73–80 (1994).
5. M. Giovagnoni, "Linear decoupled models for a slewing beam undergoing large rotations," *J. Sound Vib.* **164**, 485–501 (1993).
6. C. Damaren and I. Sharf, "Simulation of flexible-link manipulators with inertial and geometric nonlinearities," *ASME J. Dyn. Syst. Meas. Control* **117**, 74–87 (1993).
7. R. Di Gregorio and V. Parenti-Castelli, "On the characterization of the dynamic performances of planar manipulators," *Meccanica* **40** 267–279 (2005).
8. H. Ali Attia "Dynamic analysis of spatial linkages: A recursive approach," *Meccanica* **40** 267–279 (2005).
9. A. C. Lee and S. T. Chen, "Collocated sensor/actuator positioning and feedback design in the control of flexible structure system," *ASME J. Vib. Acoust.* **116**, 146–154 (1994).
10. J. H. Park and H. Asada, "Dynamic Analysis of noncollocated flexible arms and design of torque transmission mechanism," *ASME J. Dyn. Syst. Meas. Control* **116**, 201–207 (1994).

11. W. J. Book, O. Miaza-Neto and D. E. Witney, "Feedback control of two beams, two joint system with distributed flexibility," *ASME J. Dyn. Syst. Meas. Control* **97**, 424–431 (1975).
12. R. F. Fung and H. H. Chen, "Dynamic analysis and vibration control of a flexible slide-crank mechanism using PM synchronous servo motor drive," *J. Sound Vib.* **204**, 605–637 (1998).
13. E. G. Christoforou and C. J. Damaren, "The control of flexible links robots manipulating large payloads," *J. Robotic Syst.* **17**, 255–271 (2000).
14. C. J. Damaren, "On the dynamics and control of flexible multibody systems with closed loops," *Int. J. Rob. Res.* **3**, 62–75 (2000).
15. A. G. Willis, D. Bates, A. J. Fleming, B. Ninness and S. O. Moheimani, "Model predictive control applied to constraints handling in active noise and vibration control," *IEEE Trans. Control Syst. Technol.* **16**(1), 3–12 (2008).
16. M. S. Fallah, S. H. Long, W. F. Xie and R. Bhat, "Robust model predictive control of shimmy vibration in aircraft landing gears," *J. Aircr.* **45**(6), 1872–1880 (2008).
17. J. Wang, Y. Zhang, L. Xu, Y. Jing and S. Zhang, "Torsional Vibration Suppression of Rolling Mill with Constrained Model Predictive Control," *Proceedings 6th World Congress on Intelligent Control and Automation*, Dalian, China (Jun. 21–23 2006) pp. 6401–6405.
18. N. O. Ghahramania and F. Towhidkhah, "Constrained incremental predictive controller design for a flexible joint robot," *ISA Trans.* **48**(3), 321–326 (2009).
19. M. Hassan, R. Dubay, C. Li and R. Wang, "Active vibration control of a flexible one-link manipulator using a multivariable predictive controller," *Mechatronics* **17**, 311–323 (2007).
20. T. Fan and C. W. De Silva, "Dynamic modelling and model predictive control of flexible-link manipulators," *Int. J. Robot. Autom.* **23**(4), pp. 227–234 (2008).
21. P. Boscariol, A. Gasparetto and V. Zanotto, "Vibration Reduction in a Single-Link Flexible Mechanism Trough the Synthesis of an MPC Controller," *Proceedings of the IEEE International Conference on Mechatronics, (ICM '09)*, Malaga, Spain (2009) pp. 1–6.
22. P. Boscariol, A. Gasparetto and V. Zanotto, "Model predictive control of a flexible links mechanism," *J. Intell. Robot. Syst.* **58**(2), 125–147 (2010).
23. R. Caracciolo, D. Richiedei, A. Trevisani and V. Zanotto, "Robust mixed-norm position and vibration control of flexible link mechanisms," *Mechatronics* **15**, 767–791 (2005).
24. R. Caracciolo and A. Trevisani, "Simultaneous rigid-body motion and vibration control of a flexible four-bar linkage," *Mech. Mach. Theory*, **36**(2), 221–243 (2001).
25. A. Gasparetto, "Accurate modeling of a flexible-link planar mechanism by means of a linearized model in the state-space form for design of a vibration control," *J. Sound Vib.* **240**(2), 241–262 (2001).
26. J. M. Maciejowski, *Predictive Control with Constraints* (Prentice Hall, Upper Saddle River, NJ, USA, 2002).
27. L. Wang, *Model Predictive Control System Design and Implementation using Matlab* (Spinger-Verlag, London, UK, 2009).
28. E. F. Camacho and C. Bordons, *Model Predictive Control* (Springer, New York, USA, 2004).